Measurements of Flavour Dependent Fragmentation Functions in $Z^0 \rightarrow q\bar{q}$ Events

The OPAL Collaboration

Abstract

Fragmentation functions for charged particles in $Z^0 \rightarrow q\bar{q}$ events have been measured for bottom (b), charm (c) and light (uds) quarks as well as for all flavours together. The results are based on data recorded between 1990 and 1995 using the OPAL detector at LEP. Event samples with different flavour compositions were formed using reconstructed $D^{*\pm}$ mesons and secondary vertices. The $\xi_p = \ln(1/x_p)$ distributions and the position of their maxima ξ_0 are also presented separately for uds, c and b quark events. The fragmentation function for b quarks is significantly softer than for uds quarks.

The OPAL Collaboration

K. Ackerstaff[8], G. Alexander[23], J. Allison[16], N. Altekamp[5], K.J. Anderson[9], S. Anderson[12],
S. Arcelli[2], S. Asai[24], S.F. Ashby[1], D. Axen[29], G. Azuelos[18,a], A.H. Ball[17], E. Barberio[8],
R.J. Barlow[16], R. Bartoldus[3], J.R. Batley[5], S. Baumann[3], J. Bechtluft[14], T. Behnke[8],
K.W. Bell[20], G. Bella[23], S. Bentvelsen[8], S. Bethke[14], S. Betts[15], O. Biebel[14], A. Biguzzi[5],
S.D. Bird[16], V. Blobel[27], I.J. Bloodworth[1], M. Bobinski[10], P. Bock[11], J. Böhme[14],
M. Boutemeur[34], S. Braibant[8], P. Bright-Thomas[1], R.M. Brown[20], H.J. Burckhart[8],
C. Burgard[8], R. Bürgin[10], P. Capiluppi[2], R.K. Carnegie[6], A.A. Carter[13], J.R. Carter[5],
C.Y. Chang[17], D.G. Charlton[1,b], D. Chrisman[4], C. Ciocca[2], P.E.L. Clarke[15], E. Clay[15],
I. Cohen[23], J.E. Conboy[15], O.C. Cooke[8], C. Couyoumtzelis[13], R.L. Coxe[9], M. Cuffiani[2],
S. Dado[22], G.M. Dallavalle[2], R. Davis[30], S. De Jong[12], L.A. del Pozo[4], A. de Roeck[8],
K. Desch[8], B. Dienes[33,d], M.S. Dixit[7], M. Doucet[18], J. Dubbert[34], E. Duchovni[26], G. Duckeck[34],
I.P. Duerdoth[16], D. Eatough[16], P.G. Estabrooks[6], E. Etzion[23], H.G. Evans[9], F. Fabbri[2],
A. Fanfani[2], M. Fanti[2], A.A. Faust[30], F. Fiedler[27], M. Fierro[2], H.M. Fischer[3], I. Fleck[8],
R. Folman[26], A. Fürtjes[8], D.I. Futyan[16], P. Gagnon[7], J.W. Gary[4], J. Gascon[18],
S.M. Gascon-Shotkin[17], C. Geich-Gimbel[3], T. Geralis[20], G. Giacomelli[2], P. Giacomelli[2],
V. Gibson[5], W.R. Gibson[13], D.M. Gingrich[30,a], D. Glenzinski[9], J. Goldberg[22], W. Gorn[4],
C. Grandi[2], E. Gross[26], J. Grunhaus[23], M. Gruwé[27], G.G. Hanson[12], M. Hansroul[8],
M. Hapke[13], C.K. Hargrove[7], C. Hartmann[3], M. Hauschild[8], C.M. Hawkes[5], R. Hawkings[27],
R.J. Hemingway[6], M. Herndon[17], G. Herten[10], R.D. Heuer[8], M.D. Hildreth[8], J.C. Hill[5],
S.J. Hillier[1], P.R. Hobson[25], A. Hocker[9], R.J. Homer[1], A.K. Honma[28,a], D. Horváth[32,c],
K.R. Hossain[30], R. Howard[29], P. Hüntemeyer[27], P. Igo-Kemenes[11], D.C. Imrie[25], K. Ishii[24],
F.R. Jacob[20], A. Jawahery[17], H. Jeremie[18], M. Jimack[1], A. Joly[18], C.R. Jones[5], P. Jovanovic[1],
T.R. Junk[8], D. Karlen[6], V. Kartvelishvili[16], K. Kawagoe[24], T. Kawamoto[24], P.I. Kayal[30],
R.K. Keeler[28], R.G. Kellogg[17], B.W. Kennedy[20], A. Klier[26], S. Kluth[8], T. Kobayashi[24],
M. Kobel[3,e], D.S. Koetke[6], T.P. Kokott[3], M. Kolrep[10], S. Komamiya[24], R.V. Kowalewski[28],
T. Kress[11], P. Krieger[6], J. von Krogh[11], P. Kyberd[13], G.D. Lafferty[16], D. Lanske[14], J. Lauber[15],
S.R. Lautenschlager[31], I. Lawson[28], J.G. Layter[4], D. Lazic[22], A.M. Lee[31], E. Lefebvre[18],
D. Lellouch[26], J. Letts[12], L. Levinson[26], R. Liebisch[11], B. List[8], C. Littlewood[5], A.W. Lloyd[1],
S.L. Lloyd[13], F.K. Loebinger[16], G.D. Long[28], M.J. Losty[7], J. Ludwig[10], D. Lui[12],
A. Macchiolo[2], A. Macpherson[30], M. Mannelli[8], S. Marcellini[2], C. Markopoulos[13],
A.J. Martin[13], J.P. Martin[18], G. Martinez[17], T. Mashimo[24], P. Mättig[26], W.J. McDonald[30],
J. McKenna[29], E.A. Mckigney[15], T.J. McMahon[1], R.A. McPherson[28], F. Meijers[8], S. Menke[3],
F.S. Merritt[9], H. Mes[7], J. Meyer[27], A. Michelini[2], S. Mihara[24], G. Mikenberg[26], D.J. Miller[15],
R. Mir[26], W. Mohr[10], A. Montanari[2], T. Mori[24], K. Nagai[26], I. Nakamura[24], H.A. Neal[12],
B. Nellen[3], R. Nisius[8], S.W. O'Neale[1], F.G. Oakham[7], F. Odorici[2], H.O. Ogren[12],
M.J. Oreglia[9], S. Orito[24], J. Pálinkás[33,d], G. Pásztor[32], J.R. Pater[16], G.N. Patrick[20], J. Patt[10],
R. Perez-Ochoa[8], S. Petzold[27], P. Pfeifenschneider[14], J.E. Pilcher[9], J. Pinfold[30], D.E. Plane[8],
P. Poffenberger[28], B. Poli[2], J. Polok[8], M. Przybycień[8], C. Rembser[8], H. Rick[8], S. Robertson[28],
S.A. Robins[22], N. Rodning[30], J.M. Roney[28], K. Roscoe[16], A.M. Rossi[2], Y. Rozen[22], K. Runge[10],

O. Runolfsson[8], D.R. Rust[12], K. Sachs[10], T. Saeki[24], O. Sahr[34], W.M. Sang[25],
E.K.G. Sarkisyan[23], C. Sbarra[29], A.D. Schaile[34], O. Schaile[34], F. Scharf[3], P. Scharff-Hansen[8],
J. Schieck[11], B. Schmitt[8], S. Schmitt[11], A. Schöning[8], T. Schorner[34], M. Schröder[8],
M. Schumacher[3], C. Schwick[8], W.G. Scott[20], R. Seuster[14], T.G. Shears[8], B.C. Shen[4],
C.H. Shepherd-Themistocleous[8], P. Sherwood[15], G.P. Siroli[2], A. Sittler[27], A. Skuja[17],
A.M. Smith[8], G.A. Snow[17], R. Sobie[28], S. Söldner-Rembold[10], M. Sproston[20], A. Stahl[3],
K. Stephens[16], J. Steuerer[27], K. Stoll[10], D. Strom[19], R. Ströhmer[34], R. Tafirout[18], S.D. Talbot[1],
S. Tanaka[24], P. Taras[18], S. Tarem[22], R. Teuscher[8], M. Thiergen[10], M.A. Thomson[8], E. von
Törne[3], E. Torrence[8], S. Towers[6], I. Trigger[18], Z. Trócsányi[33], E. Tsur[23], A.S. Turcot[9],
M.F. Turner-Watson[8], R. Van Kooten[12], P. Vannerem[10], M. Verzocchi[10], P. Vikas[18], H. Voss[3],
F. Wäckerle[10], A. Wagner[27], C.P. Ward[5], D.R. Ward[5], P.M. Watkins[1], A.T. Watson[1],
N.K. Watson[1], P.S. Wells[8], N. Wermes[3], J.S. White[28], G.W. Wilson[14], J.A. Wilson[1],
T.R. Wyatt[16], S. Yamashita[24], G. Yekutieli[26], V. Zacek[18], D. Zer-Zion[8]

[1]School of Physics and Astronomy, University of Birmingham, Birmingham B15 2TT, UK
[2]Dipartimento di Fisica dell' Università di Bologna and INFN, I-40126 Bologna, Italy
[3]Physikalisches Institut, Universität Bonn, D-53115 Bonn, Germany
[4]Department of Physics, University of California, Riverside CA 92521, USA
[5]Cavendish Laboratory, Cambridge CB3 0HE, UK
[6]Ottawa-Carleton Institute for Physics, Department of Physics, Carleton University, Ottawa, Ontario K1S 5B6, Canada
[7]Centre for Research in Particle Physics, Carleton University, Ottawa, Ontario K1S 5B6, Canada
[8]CERN, European Organisation for Particle Physics, CH-1211 Geneva 23, Switzerland
[9]Enrico Fermi Institute and Department of Physics, University of Chicago, Chicago IL 60637, USA
[10]Fakultät für Physik, Albert Ludwigs Universität, D-79104 Freiburg, Germany
[11]Physikalisches Institut, Universität Heidelberg, D-69120 Heidelberg, Germany
[12]Indiana University, Department of Physics, Swain Hall West 117, Bloomington IN 47405, USA
[13]Queen Mary and Westfield College, University of London, London E1 4NS, UK
[14]Technische Hochschule Aachen, III Physikalisches Institut, Sommerfeldstrasse 26-28, D-52056 Aachen, Germany
[15]University College London, London WC1E 6BT, UK
[16]Department of Physics, Schuster Laboratory, The University, Manchester M13 9PL, UK
[17]Department of Physics, University of Maryland, College Park, MD 20742, USA
[18]Laboratoire de Physique Nucléaire, Université de Montréal, Montréal, Quebec H3C 3J7, Canada
[19]University of Oregon, Department of Physics, Eugene OR 97403, USA
[20]Rutherford Appleton Laboratory, Chilton, Didcot, Oxfordshire OX11 0QX, UK
[22]Department of Physics, Technion-Israel Institute of Technology, Haifa 32000, Israel
[23]Department of Physics and Astronomy, Tel Aviv University, Tel Aviv 69978, Israel
[24]International Centre for Elementary Particle Physics and Department of Physics, University

of Tokyo, Tokyo 113, and Kobe University, Kobe 657, Japan

[25]Institute of Physical and Environmental Sciences, Brunel University, Uxbridge, Middlesex UB8 3PH, UK

[26]Particle Physics Department, Weizmann Institute of Science, Rehovot 76100, Israel

[27]Universität Hamburg/DESY, II Institut für Experimental Physik, Notkestrasse 85, D-22607 Hamburg, Germany

[28]University of Victoria, Department of Physics, P O Box 3055, Victoria BC V8W 3P6, Canada

[29]University of British Columbia, Department of Physics, Vancouver BC V6T 1Z1, Canada

[30]University of Alberta, Department of Physics, Edmonton AB T6G 2J1, Canada

[31]Duke University, Dept of Physics, Durham, NC 27708-0305, USA

[32]Research Institute for Particle and Nuclear Physics, H-1525 Budapest, P O Box 49, Hungary

[33]Institute of Nuclear Research, H-4001 Debrecen, P O Box 51, Hungary

[34]Ludwigs-Maximilians-Universität München, Sektion Physik, Am Coulombwall 1, D-85748 Garching, Germany

[a] and at TRIUMF, Vancouver, Canada V6T 2A3

[b] and Royal Society University Research Fellow

[c] and Institute of Nuclear Research, Debrecen, Hungary

[d] and Department of Experimental Physics, Lajos Kossuth University, Debrecen, Hungary

[e] on leave of absence from the University of Freiburg

1 Introduction

Experimental measurements of the inclusive momentum distribution of charged particles in e^+e^- collisions provide important insight into the process of how quarks turn into hadrons. This distribution is commonly normalised to the total hadronic cross section σ^{tot} and presented as a function of the scaled momenta $x_p = 2p_h/\sqrt{s}$ of the charged hadrons, where $\sqrt{s}$ is the centre-of-mass energy. In this form, the spectrum is usually referred to as the fragmentation function and can be obtained experimentally from the total number of hadronic final states, N_{event}, and the number of charged particles in each x_p bin, $N_{\mathrm{track}}(x_p)$:

$$F(x_p) = \frac{1}{\sigma^{\mathrm{tot}}} \frac{\mathrm{d}\sigma^h}{\mathrm{d}x_p} = \frac{1}{N_{\mathrm{event}}} \frac{N_{\mathrm{track}}(x_p)}{\Delta x_p}. \tag{1}$$

The charged particle momentum spectrum can also be studied as the distribution of $\xi_p = \ln(1/x_p)$. The ξ_p distribution emphasises the low momentum component and the x_p distribution the high momentum component of the momentum spectrum.

In the naïve quark parton model, the scaled momentum distribution is expected to be independent from the centre-of-mass energy. A violation of this scaling is expected due to gluon radiation in the final state. Experimentally, scaling violation in fragmentation functions had indeed been observed by combining measurements at different centre-of-mass energies and could be used to determine α_s [1]. The position of the maximum of the ξ_p distribution, ξ_0, has been studied in the past in various experiments (see for example [2] and references therein). The energy dependence of the position of the maximum provides an important test of the QCD prediction for the emission of soft gluons [3].

In events with a heavy primary quark, the possibility of cascade decays of bottom or charm hadrons results in more particles sharing the same energy than in light quark events and a softer momentum spectrum can be expected. Since the flavour composition of the primary quarks in $e^+e^- \to q\bar{q}$ is predicted by the electroweak theory to change with centre-of-mass energy, this flavour dependence of the momentum spectra affects the energy dependence of the x_p and ξ_p distributions of the inclusive event sample. To correct for this contribution, in [4] not only the inclusive fragmentation function was measured but also fragmentation functions in event samples with different flavour compositions were studied. In [5], measurements of fragmentation functions in samples with different flavour composition were used to extract flavour dependent fragmentation functions for events with primary light (uds), charm (c) or bottom (b) quarks.

Here we present a measurement of flavour dependent fragmentation functions, based on the methods developed for the OPAL measurement of charged particle multiplicities in uds, c and b quark events [6, 7]. Events were divided into two hemispheres by a plane perpendicular to the thrust axis. Secondary vertices and reconstructed $D^{*\pm}$ mesons were used to tag hemispheres to create samples of events with different quark flavour mixtures (Section 2). To reduce the biases induced by the tagging, the measurement of the fragmentation functions was based on the momentum spectrum of charged particles in the event hemisphere opposite to the tag. Corrections for hemisphere correlations and for distortions due to detector effects are described in Section 3. The flavour dependent x_p and ξ_p distributions were obtained from a simultaneous

fit to the momentum spectra of the different hemisphere samples (Section 4). For the first time, the measured position of the maximum of the ξ_p distribution, ξ_0, is presented separately for uds, c and b events. A measurement of the inclusive distribution of all five flavours was also performed, based on the track momentum spectrum of all events, i.e., without considering any flavour tagging.

2 Selection and event tagging

A complete description of the OPAL detector can be found elsewhere [8]. This analysis relied on the precise reconstruction of charged particles in the central detector, consisting of a silicon microvertex detector, a vertex drift chamber, a large volume jet chamber and chambers measuring the z-coordinate[1] of tracks as they leave the jet chamber.

This analysis used data recorded with the OPAL detector in the years 1990 to 1995 at centre-of-mass energies around 91.2 GeV comprising an integrated luminosity of about 177 pb^{-1}. Z^0 decays were selected using the criteria described in [9]. To ensure that most charged particles were well contained in the detector, the polar angle of the thrust axis was required to satisfy $|\cos\theta_{\text{thrust}}| < 0.8$. To reduce systematic errors in the application of the secondary vertex tag, it was only based on a homogeneous data sample taken in the year 1994, representing an integrated luminosity of about 34 pb^{-1}. The full integrated luminosity was used in the case of the D$^{*\pm}$ meson tag.

Charged tracks used in the measurement of the fragmentation function were required to have a measured momentum in the x-y plane, p_t, of at least 0.150 GeV/c and to satisfy $|d_0| < 0.5$ cm, where d_0 is the distance of closest approach to the origin in the x-y plane.

Simulated hadronic Z^0 decays were generated with the Jetset 7.4 Monte Carlo program [10] tuned to OPAL data [11]. The events were passed through a detailed simulation of the OPAL detector [12] and processed using the same reconstruction and selection algorithms as the data.

2.1 Secondary vertex tag

Samples with varying purity of b quark events were selected by reconstructing secondary vertices, following the procedure described in [6]. Events were divided into two hemispheres by the plane perpendicular to the thrust axis and comprising the interaction point. Jets were reconstructed by combining charged tracks and electromagnetic clusters not associated to tracks, using the scaled invariant mass algorithm described in [13] with the JADE-E0 recombination scheme and the invariant mass cut-off being set to $7\,\text{GeV}/c^2$. A vertex fit was then attempted in the highest energy jet in each hemisphere separately. Each track used in these vertex fits was required to have at least one hit in the silicon microvertex detector. All

---

[1]The OPAL coordinate system is defined with positive z along the electron beam direction and with positive x pointing towards the centre of the LEP ring. The polar angle θ is defined relative to the $+z$ axis and the azimuthal angle ϕ relative to the $+x$ axis.

such tracks in the jet were fitted to a common vertex point in the x-y plane and the track with the largest contribution to the χ^2 was removed if this contribution was greater than four. The remaining tracks were then refitted until either all tracks contributed less than four to the χ^2 or there were fewer than four remaining tracks. For each successfully reconstructed secondary vertex, the projected decay length L in the x-y plane with respect to the primary vertex was calculated, where the primary vertex was reconstructed from all tracks in the event together with a constraint to the average beamspot position as in [14].

The decay length significance, i.e. the decay length divided by its uncertainty L/σ_L was used to obtain three event samples k of varying b flavour purity. According to the simulation, the b purities f_k^{b} in these samples vary from 11% to 90% (see Table 1). Fig 1(a) shows the distribution of the decay length significance in data and in Monte Carlo.

	$-10.0 < L/\sigma_L < 1.0$	$1.0 < L/\sigma_L < 5.0$	$5.0 < L/\sigma_L < 50.0$
Number of hemispheres	940 275	268 500	117 665
uds quark fraction f_k^{uds}	0.71	0.39	0.04
c quark fraction f_k^{c}	0.18	0.23	0.06
b quark fraction f_k^{b}	0.11	0.38	0.90

Table 1: *Number of tagged hemispheres in data and the flavour composition derived from the Monte Carlo simulation in three decay length significance regions.*

2.2 D$^{*\pm}$ meson tag

Event samples with an enriched c quark contribution were obtained by reconstructing D$^{*\pm}$ meson candidates. D$^{*\pm}$ candidates were selected via the decay[2] D$^{*+} \to$ K$^-\pi^+\pi^+$ closely following the procedure described in [7]:

- A subset of tracks was selected that have $p_t > 0.250$ GeV/c and $|d_0| < 0.5$ cm.

- Candidates of D$^0 \to$ K$^-\pi^+$ decays were selected by taking all combinations of two oppositely charged tracks, with one of them assumed to be a pion and the other assumed to be a kaon. D$^{*\pm}$ candidates were selected by combining D^0 candidates with a third track. This 'slow pion' track was required to have the same charge as the track presumed to be the pion in the D^0 decay.

- The probability that the measured rate of energy loss, dE/dx, for the kaon candidate track was consistent with that expected for a real kaon was required to be greater than 10%.

- At least two of the three tracks were required to have either z-chamber hits or a polar angle measurement derived from the point at which the track has left the jet chamber.

---

[2]Throughout this paper, charge conjugate particles and decay modes are always implied.

- The invariant mass of the D^0 candidate was required to be between $1.790\,\mathrm{GeV}/c^2$ and $1.940\,\mathrm{GeV}/c^2$ and the mass difference between the D^0 and the $D^{*\pm}$ candidate, ΔM, was required to be between $0.142\,\mathrm{GeV}/c^2$ and $0.149\,\mathrm{GeV}/c^2$.

- Making use of the fact that real D^0 mesons decay isotropically in their rest frames whereas combinatorial background is peaked in the forward and the backward direction, the following cuts were applied: $|\cos\theta^*| < 0.8$ for $x_{D^*} < 0.5$ and $|\cos\theta^*| < 0.9$ for $x_{D^*} > 0.5$, where θ^* is the angle between the kaon in the D^0 rest frame and the direction of the D^0 in the laboratory frame and x_{D^*} is the scaled energy of the $D^{*\pm}$, i.e., $x_{D^*} = 2E_{D^{*\pm}}/\sqrt{s}$.

To provide samples with differing charm purity, the data were divided into three x_{D^*} regions. To evaluate their flavour composition, ΔM distributions obtained without the cut on ΔM were fitted with a Gaussian for the signal and a function $A\exp(-B\Delta M)(\Delta M/m_\pi - 1)^C$ for the background [15]. The signals, together with the fitted functions are shown in Fig. 1(b)-(d). These fits were used to determine the fraction of background, f_k^{BG} in each $D^{*\pm}$ sample in the signal ΔM region. The results of these fits are summarised in Table 2.

	$0.2 < x_{D^*} < 0.4$	$0.4 < x_{D^*} < 0.6$	$0.6 < x_{D^*} < 1.0$
Number of $D^{*\pm}$ candidates	5109	1951	985
combinatorial background fraction f_k^{BG}	0.57	0.36	0.24
c quark fraction $\mathcal{P}_k^{\mathrm{c}}$	0.22 ± 0.06	0.50 ± 0.06	0.90 ± 0.04
b quark fraction $\mathcal{P}_k^{\mathrm{b}}$	0.78 ± 0.06	0.50 ± 0.06	0.10 ± 0.04

Table 2: *Number of* $D^{*\pm}$ *candidates, the fitted background fraction and the flavour composition of events with a genuine* $D^{*\pm}$ *as taken from [15] in three* x_{D^*} *regions.*

The selected samples of $D^{*\pm}$ candidates have three components: genuine $D^{*\pm}$ mesons from b quark decays, genuine $D^{*\pm}$ mesons from c quark decays and combinatorial background. No other sources of $D^{*\pm}$ candidates were considered since Monte Carlo simulations predicts that only 0.3% of $D^{*\pm}$ mesons with $x_{D^*} > 0.2$ are produced via gluon splitting in light quark events [15]. To evaluate the effect of the contribution from fake $D^{*\pm}$, a side-band sample was selected by requiring that the two pions of the $D^{*\pm}$ candidates had opposite charge and that $0.150\ \mathrm{GeV}/c^2 < \Delta M < 0.170\ \mathrm{GeV}/c^2$. Once this contribution was taken into account, the flavour composition of the $D^{*\pm}$ samples was taken as the fractions $\mathcal{P}_k^{\mathrm{c}}$ and $\mathcal{P}_k^{\mathrm{b}}$ of genuine $D^{*\pm}$ mesons originating from a primary c quark and b quark as measured in [15]. While in [15] the fractions $\mathcal{P}_k^{\mathrm{c}}$ and $\mathcal{P}_k^{\mathrm{b}}$ were derived for $D^{*\pm}$ candidates after corrections for detector efficiency and acceptance were made, they were applied in this analysis to uncorrected data. No modifications were made since tests with Monte Carlo simulated events showed no significant flavour dependence of these corrections.

3 Corrections

The track momentum distributions in the hemispheres opposite to the secondary vertex or $D^{*\pm}$ tag were measured. Six distributions (label k) were obtained, corresponding to the three decay length regions and the three x_{D^*} regions. To obtain fragmentation functions from these distributions, three sets of corrections were applied. Firstly, a correction was made to take into account track momentum resolution and reconstruction efficiency. Secondly, the effects due to the event selection and the correlation between hemispheres were accounted for. In addition, the measured track momentum spectra in the $D^{*\pm}$ tag samples were corrected for the contribution of fake $D^{*\pm}$ mesons. The different corrections are described in the following.

After this procedure, the track momentum distributions are defined as the momentum distributions of all promptly produced stable charged particles and those produced in the decays of particles with lifetimes shorter than 3×10^{-10} sec., corrected for initial state radiation. This means that charged decay products from K_s^0, hyperons and weakly decaying b and c flavoured hadrons are included in the definition, regardless of how far away from the interaction point the decay actually occurred.

3.1 Track momentum resolution and efficiency

The number $N_{j,k}^{\text{observed}}$ of tracks in a tag sample was measured in 22 different x_p bins j.[3] The corrected distribution for a given tag sample is

$$N_{i,k}^{\text{corrected}} = \sum_j \sum_q \frac{\mathcal{M}_{ij}^q}{\epsilon_i^q} (w_{j,k}^q N_{j,k}^{\text{observed}}). \tag{2}$$

Here, $\mathcal{M}_{ij}^q$ is the probability that a track measured in x_p bin j originates from a true x_p bin i. This correction was applied to account for the migration of the tracks between different bins due to the track momentum resolution. The reconstruction efficiency for tracks belonging to a true x_p bin i is accounted for by factors ϵ_i^q. Differences in the slope of the x_p spectrum between uds, c and b quark events lead to flavour dependent migration effects and to a flavour dependent efficiency. Consequently, the matrix $\mathcal{M}_{ij}^q$ and ϵ_i^q are flavour dependent and have to be applied to the fraction $w_{j,k}^q$ of observed tracks created in a $q = $ uds, c or b event.

These weights $w_{j,k}^q$ are the normalised products of the flavour dependent fragmentation function F_j^q in an x_p bin j and the fraction f_k^q of events of a primary quark q in the considered tag sample:

$$w_{j,k}^q = \frac{f_k^q F_j^q}{\sum_{q'} f_k^{q'} F_j^{q'}}. \tag{3}$$

The applied weights and the obtained fragmentation functions are strongly correlated. This was taken into account in an iterative procedure, whereby the result of the measurement was used to re-calculate $w_{j,k}^q$ and to repeat the correction procedure until the results were stable.

---

[3]For the measurement of the ξ_p distribution, a different binning with 29 ξ_p bins was used. Apart from the binning, there were no differences between the analysis of the x_p and the ξ_p distribution, so the measurement of the ξ_p distribution is not explicitly described in the following sections.

Initial values for the weighting factors were taken from Monte Carlo, but alternative initial values were also tried to confirm that the results did not depend on the choice of the initial values.

The values for $\mathcal{M}_{ij}^q$ and ϵ_i^q were obtained from Monte Carlo. The diagonal elements $\mathcal{M}_{ii}^q$ of the matrix, i.e., the probability that a track measured in its true x_p bin is around 80% in most bins, but becomes significantly smaller for high x_p bins in c and b flavoured events. Values for the efficiency are typically around $\epsilon_i^q \approx 90\%$ with the exception of the lowest x_p bin where the efficiency is about 50%. The efficiency shows only a weak flavour dependence, the values differ for different flavours by less than 5%.

The corrected number of tracks $N_{i,k}^{\text{corrected}}$ in each tag sample was divided by the corresponding number of tagged hemispheres N_k^{hemi} to form a fragmentation function for each tagged sample:

$$\mathcal{F}_{i,k} = \frac{N_{i,k}^{\text{corrected}}}{N_k^{\text{hemi}}}. \tag{4}$$

3.2 Flavour tagging and hemisphere correlations

D$^{*\pm}$ mesons with high values of x_{D^*} and secondary vertices with large values for the decay length significance L/σ_L are more likely to be found in high energy jets. The hemisphere containing the highest energy jet also tends to have a higher charged particle multiplicity and a harder track momentum spectrum than the opposite hemisphere. Consequently, the measured fragmentation functions in samples with high values for L/σ_L or x_{D^*} would be too soft. To correct for this bias, the whole analysis was performed separately for the case where the tag-hemisphere contains the highest energy jet and where this is not the case. The unweighted average of the two results was taken at the end.

The dependence of the track momentum spectrum on the actual value of the decay length significance and on the D$^{*\pm}$ energy was also considered. Requiring a high value for L/σ_L or x_{D^*} reduces the phase space for gluon bremsstrahlung and thus introduces a kinematic correlation between the hemispheres. The effect is flavour dependent, becoming more important for higher values of x_p and is more pronounced for the D$^{*\pm}$ tag than for the secondary vertex tag. Besides this kinematical effect, correlations also occur due to geometrical effects: in a typical two jet event, the jets are back to back, thus pointing into geometrically opposite parts of the detector. This introduces a hemisphere correlation if the detector response is not uniform. In addition to the kinematical and the geometrical correlations, the difference in the fragmentation functions in tagged events and in unselected events had to be taken into account.

All these effects were accounted for by applying correction factors for each tag sample, flavour and x_p bin:

$$\mathcal{T}_{i,k}^q = \frac{F_{i,k}^q(\text{generated})}{F_i^q(\text{generated})}, \tag{5}$$

i.e., the ratio of the generated fragmentation functions in tagged events and in events where the tag has not been applied. These correction factors $\mathcal{T}$ lead to a 10% correction for high

9

x_p values opposite a hemisphere tagged by a secondary vertex and up to a 50% correction for high x_p values opposite a $D^{*\pm}$ tagged hemisphere. Technically, these factors are applied as corrections to the purities in the fit procedure, thus taking into account the *a priori* unknown flavour composition of the tracks in a specific x_p bin.

3.3 Background subtraction in the $D^{*\pm}$ samples

The measured fragmentation functions in the $D^{*\pm}$ signal samples $\mathcal{F}_{i,k}^{\mathrm{signal}}$ and the side-band samples $\mathcal{F}_{i,k}^{\mathrm{SB}}$ were used to determine the fragmentation functions for genuine $D^{*\pm}$ mesons:

$$\mathcal{F}_{i,k}^{\mathrm{D}^{*\pm}} = \frac{1}{(1 - f_k^{\mathrm{BG}})} \left(\mathcal{F}_{i,k}^{\mathrm{signal}} - f_k^{\mathrm{BG}} c_{i,k} \mathcal{F}_{i,k}^{\mathrm{SB}} \cdot \right) \tag{6}$$

The background fractions f_k^{BG} derived from fits to the ΔM distribution are listed in table 2. To take into account differences of the hemisphere correlations for events in the signal and those in the side-band region, correction factors $c_{i,k} = \mathcal{T}_{i,k}^{\mathrm{signal}}/\mathcal{T}_{i,k}^{\mathrm{SB}}$ were applied to the fragmentation functions of the side-band samples, i.e., they were multiplied by the ratio of the correction factors $\mathcal{T}$ for the flavour mix of the signal and the side-band sample as predicted by the simulation.

4 Fits

A simultaneous fit was performed on the fragmentation functions $\mathcal{F}_{i,k}^{\mathrm{D}^{*\pm}}$ and $\mathcal{F}_{i,k}^{\mathrm{vtx}}$ of the three $D^{*\pm}$ and the three secondary vertex tagged samples to extract the flavour dependent fragmentation functions F^{uds}, F^{c} and F^{b}. The fragmentation functions obtained from samples tagged by $D^{*\pm}$ decays $\mathcal{F}_{i,k}^{\mathrm{D}^{*\pm}}$, corrected for detector effects and for the combinatorial background for each of the three x_{D^*} regions k and each of the 22 x_p bins i were described in the fit by

$$\mathcal{F}_{i,k}^{\mathrm{D}^{*\pm}} = (\mathcal{P}_k^{\mathrm{c}} \mathcal{T}_{i,k}^{q=\mathrm{c}}) F_i^{\mathrm{c}} + (\mathcal{P}_k^{\mathrm{b}} \mathcal{T}_{i,k}^{q=\mathrm{b}}) F_i^{\mathrm{b}}, \tag{7}$$

where the purities $\mathcal{P}_k^{\mathrm{c}}$, $\mathcal{P}_k^{\mathrm{b}}$ are given in Table 2 and the correction factors $\mathcal{T}_{i,k}^q$ are defined in equation 5. Naïvely, the fragmentation function corrected for detector effects for each of the three samples tagged by secondary vertices and each of the 22 x_p bins could be described by

$$\mathcal{F}_{i,k}^{\mathrm{vtx}} = (f_k^{uds} \mathcal{T}_{i,k}^{q=\mathrm{uds}}) F_i^{\mathrm{uds}} + (f_k^{c} \mathcal{T}_{i,k}^{q=\mathrm{c}}) F_i^{\mathrm{c}} + (f_k^{b} \mathcal{T}_{i,k}^{q=\mathrm{b}}) F_i^{\mathrm{b}}. \tag{8}$$

However, the fraction of c events f_k^{c} in all three vertex tagged samples is small (see Table 1), hence the relative uncertainty on these fractions large. If equation 8 would be used, the vertex tagged samples would dominate the fit results due to their larger statistical weight as compared to the $D^{*\pm}$ tagged samples. To ensure that the $D^{*\pm}$ samples are used to obtain the charm fragmentation function, the flavour fraction f_k^{uds} and f_k^{c} were replaced by $(1 - f_k^b)R_{\mathrm{uds}}/(R_{\mathrm{uds}} + R_{\mathrm{c}})$ and $(1 - f_k^b)R_{\mathrm{c}}/(R_{\mathrm{uds}} + R_{\mathrm{c}})$ where R_{uds} and R_{c} are the Standard Model values for the branching fractions $R_q = \Gamma(Z^0 \to q\bar{q})/\Gamma(Z^0 \to \mathrm{hadrons})$. The decay length dependence of the ratio of uds to c events were accounted for by correction factors $d_{i,k}$ to the

10

measured fragmentation function. The fragmentation function of the secondary vertex tagged samples was then described by

$$d_{i,k}\mathcal{F}_{i,k}^{\text{vtx}} = (1 - (f_k^{\text{b}}\mathcal{T}_{i,k}^{q=\text{b}}))F_i^{\text{udsc}} + (f_k^{\text{b}}\mathcal{T}_{i,k}^{q=\text{b}})F_i^{\text{b}}, \tag{9}$$

where

$$F^{\text{udsc}} = \frac{R_{\text{uds}}F_i^{\text{uds}} + R_{\text{c}}F_i^{\text{c}}}{R_{\text{uds}} + R_{\text{c}}}. \tag{10}$$

The correction factors $d_{i,k}$ were derived from the momentum spectrum in Monte Carlo events with the ratio of uds to c events taken to be the same in all vertex samples, divided by the unmodified momentum spectrum with a variable ratio of uds to c events. These correction are of the order of 1% for most of the x_p bins except for the highest x_p bins where they exceed 10%.

A simultaneous fit was performed to extract F^{uds}, F^{c} and F^{b}. In fact, the secondary vertex data using equation 9 essentially fixes F^{udsc} and F^{b} and then the D$^{*\pm}$ data provide F^{c} through equation 7, allowing equation 10 to give F^{uds}. The fit was based on the track momentum spectrum of the hemisphere opposite the tag. Therefore, the results had to be multiplied by a factor of two to obtain the full event fragmentation functions as they are shown in Fig. 2 and in Table 3. The mean values of these distributions and their statistical uncertainty are:

$$\langle x_p \rangle^{\text{uds}} = 0.0630 \pm 0.0003$$
$$\langle x_p \rangle^{\text{c}} \quad = 0.0576 \pm 0.0012$$
$$\langle x_p \rangle^{\text{b}} \quad = 0.0529 \pm 0.0001.$$

The results can be compared with results for the inclusive fragmentation function which was obtained from the track momentum spectrum of all events without considering any flavour tagging. These results are shown in Table 4 and the mean value of the distribution was found to be:

$$\langle x_p \rangle^{\text{incl}} = 0.05938 \pm 0.00002.$$

The results for the ξ_p distribution are shown if Fig.3 and Table 5. To determine the positions of the maxima, ξ_0, skewed Gaussians, i.e., combinations of two Gaussians with different widths to the left and to the right from the centre were fitted to these distribution as motivated by the next-to-leading-log (NLLA) approximation [3]. Following the procedure in [17], the fit was performed in the region $2.2 < \xi_p < 5.0$. The results for the positions of the maxima with their statistical uncertainties are:

$$\xi_0{}^{\text{uds}} = 3.74 \pm 0.06$$
$$\xi_0{}^{\text{c}} \quad = 3.63 \pm 0.16$$
$$\xi_0{}^{\text{b}} \quad = 3.55 \pm 0.01.$$

Again, these flavour dependent results can be compared with the results of the inclusive ξ_p distribution as obtained from all events without any flavour tagging. The results are shown in Table 6, the position of the maximum was determined to be:

$$\xi_0{}^{\text{incl}} = 3.656 \pm 0.003 .$$

5 Systematic errors and cross checks

The systematic uncertainties affecting the above results are due to the following sources: (1) uncertainties of the purities of the samples tagged by secondary vertices and (2) by $D^{*\pm}$ decays, the $D^{*\pm}$ reconstruction (3), the hemisphere correlation (4), uncertainties inherent to the correction procedure (5) and the track and event selection (6). These were estimated from the difference between the central value and the result of the repeated analysis after a cut, a purity or the correction procedure was modified. In each case, the largest deviation was taken as the systematic error.

(1) The uncertainties on the purities in the secondary vertex event samples were estimated using the published results from the measurement of the charged multiplicity in b, c and uds events [7]. There, variations of the measured multiplicity due to the uncertainties in the b lifetime, the fragmentation of b and c quark events, the production rates and the mixture of b hadrons produced as well as the decay multiplicities were studied and can be used to derive the uncertainties on the purities. The secondary vertex sample purities were then varied in the range of their uncertainty and the resulting differences of the results for the fragmentation function was taken as the systematic error due to this source.

(2) The purities $\mathcal{P}_k^c$ and $\mathcal{P}_k^b$ of the $D^{*\pm}$ tag bins were taken from [15]. They were modified within their systematic errors to obtain the contribution to the systematic uncertainty on the fragmentation function.

(3) To study the impact of the details of the $D^{*\pm}$ candidate selection, the analysis was repeated with four sets of modified selection criteria. The $M_{D^0}^{cand}$ mass window was increased to 1.765 GeV/c^2 < $M_{D^0}^{cand}$ < 1.965 GeV/c^2; the ΔM window was increased to 0.141 GeV/c^2 < ΔM < 0.150 GeV/c^2; only one of the three tracks was required to have a z-chamber or jet chamber end point z measurement and the cuts based on dE/dx were removed. The last modification lead to a reduction of the signal to noise ratio of more than 25%.

(4) The correlation between hemispheres caused by the kinematic of gluon radiation is corrected for by the factors $\mathcal{T}$ (equation 5) . A good description of the energy spectrum and the angular distribution of jets in the Monte Carlo simulation is important for a reliable prediction of this effect. To estimate the effects of small discrepancies between data and simulation in these distribution, the analysis was repeated applying weights to Monte Carlo events so that the energy distribution of the most energetic jet and the distribution of the angle between the two most energetic jets in data and Monte Carlo simulation agreed. Most of the resulting event weights had values between 0.95 and 1.05. The difference of the results with and without weighting was taken as the systematic uncertainty.

(5) To estimate systematic uncertainties due to the correction for track momentum resolution and efficiency (Section 3.1) and corrections applied in the fitting procedure (Section 4), the following two modifications to the correction procedure were tested. First, the

weighting factors $w_{j,k}^q$ as defined in equation 3 were not re-calculated in an iterative procedure but were based on the initial values from the Monte Carlo simulation. Secondly, the correction factors $d_{i,k}$ in equation 9 were omitted, i.e., the secondary vertex samples were not corrected for the variation of the uds to c flavour fraction.

(6) To account for imperfections in the tracking detector simulation, results were obtained in six different ways with modified event and track selections and variations of track quantities in the Monte Carlo simulation. The cut on the angle of the thrust axis $|\cos\theta_{\mathrm{thrust}}| > 0.8$ was removed; instead of accepting all tracks, a cut on $|\cos\theta_{\mathrm{track}}| < 0.7$ was applied; tracks were rejected if their z-coordinate at the point of closest approach to the event origin was larger than $|z_0| > 10\,\mathrm{cm}$; tracks were rejected if their momentum was smaller than $0.250\,\mathrm{GeV}/c$; the track momenta in simulated events were modified by an additional smearing factor leading to a degradation of the momentum resolution in Monte Carlo events of 10%; the simulated track momenta were shifted by 1%. Since these effects are flavour independent, the uncertainty due to the track and event selection has been set to be the same for the inclusive and the flavour dependent fragmentation functions.

The systematic uncertainties from the above groups of effects were added in quadrature and are shown for the flavour dependent distributions in the last column of Tables 3 and 5. The result for the inclusive fragmentation function was obtained without flavour tagging and consequently does not depend on the tagging efficiency, purity or hemisphere correlation, so only the last two groups of effects contributed to the systematic uncertainty shown in the last column of Tables 4 and 6. For most of the x_p range, the relative systematic error is below 5% for uds and b events and below 10% for c events. For very high momenta ($x_p > 0.5$), the systematic uncertainty becomes larger. Note that in uds and c events, the systematic and statistical errors are roughly equal. Detailed results are shown in Table 7 for a typical low momentum x_p bin ($0.05 < x_p < 0.06$) and a typical high momentum x_p bin ($0.3 < x_p < 0.4$).

In Table 8, the systematic uncertainties on the measurement of the mean value $\langle x_p \rangle$ of the x_p distributions are shown. Further systematic checks were done for the determination of the position of the maximum of the ξ_p distributions, ξ_0. Instead of evaluating the position of the maximum using a skewed Gaussian fit, a normal Gaussian fit as motivated by LLA [18] was used. Furthermore, the fit range was modified and the skewed Gaussian was fitted to the measured ξ_p distribution in the regions $2.0 < \xi_p < 5.2$ and $2.4 < \xi_p < 4.8$. The uncertainty obtained from this test has been added in quadrature to the previous six contributions as listed in Table 9.

To cross-check the results, the tagging methods were modified. An alternative b tag was applied, based on impact parameter information rather than on decay length information: The third largest impact parameter of a track was taken as the tag quantity. The impact parameter distribution of tracks from a decay are independent from the energy of the decaying particle while the decay length of a particle is proportional to its energy. Hence, this simple alternative method is less affected by kinematical correlations due to gluon radiation but affected by other systematic effects than the standard method. The result obtained with the alternative b tagging method is consistent with the central values within the assigned systematic error. Another cross-check was performed using an alternative background treatment

13

in the $D^{*\pm}$ tagged event samples. Instead of taking the $D^{*\pm}$ purities from [15] and subtracting the effect of the combinatorial background with the help of a fit to the $D^{*\pm}$ signal, purities and background were taken from Monte Carlo. Again, the results obtained with this alternative method and the central values agreed within the systematic errors.

Effects from the binning in the tag variable have also been cross-checked. Instead of using three secondary vertex bins and three $D^{*\pm}$ bins, alternative results were obtained using two and four secondary vertex bins and likewise two and four $D^{*\pm}$ bins. The deviations from the central value were in all cases smaller than the estimated systematic error.

The whole analysis procedure has also been tested globally with simulated events. It was shown that the generated fragmentation function and the result of the unfolding procedure agree within the statistical uncertainty.

By integrating the fragmentation functions, the charged multiplicity in uds, c and b events can be obtained. The results,

$$
\begin{aligned}
n^{\text{uds}} &= 20.25 \pm 0.11 \pm 0.37 \\
n^{\text{c}} &= 21.55 \pm 0.37 \pm 0.64 \\
n^{\text{b}} &= 23.16 \pm 0.02 \pm 0.45 \\
n^{\text{incl}} &= 21.16 \pm 0.01 \pm 0.21 \,,
\end{aligned}
$$

are in good agreement with results of direct measurements of the charged multiplicities [6, 7, 23, 24].

The average of the three flavour dependent fragmentation functions can be formed, weighted with the Standard Model branching fractions R_{uds}, R_{c} and R_{b}. This combined fragmentation function can be compared with the results for the inclusive fragmentation function and with previously published OPAL results [23]. All three results show good agreement with each other.

6 Results

The results for the flavour dependent fragmentation functions for uds, c and b events as well as the inclusive fragmentation function are shown in Fig. 2 and in Tables 3 and 4. The mean values of these distributions are:

$$
\begin{aligned}
\langle x_p \rangle^{\text{uds}} &= 0.0630 \pm 0.0003 \pm 0.0011 \\
\langle x_p \rangle^{\text{c}} &= 0.0576 \pm 0.0012 \pm 0.0016 \\
\langle x_p \rangle^{\text{b}} &= 0.0529 \pm 0.0001 \pm 0.0013 \\
\langle x_p \rangle^{\text{incl}} &= 0.05938 \pm 0.00002 \pm 0.00057 \,.
\end{aligned}
$$

The light quark fragmentation function is found to be harder than the b quark fragmentation function as expected due to the cascade decays of b hadrons in b quark events with more particles sharing the energy. This observation is also consistent with the results of comparisons of gluon, uds and b jets [21, 22].

14

In Fig. 3 and in Tables 5 and 6, the results are presented for the $\xi_p = \ln(1/x_p)$ distribution which emphasises the lower momenta of the spectrum. Skewed Gaussians were fitted to these distributions to obtain the position of their maxima:

$$
\begin{aligned}
\xi_0^{\mathrm{uds}} &= 3.74 \pm 0.06 \pm 0.21 \\
\xi_0^{\mathrm{c}} &= 3.63 \pm 0.16 \pm 0.31 \\
\xi_0^{\mathrm{b}} &= 3.55 \pm 0.01 \pm 0.07 \\
\xi_0^{\mathrm{incl}} &= 3.656 \pm 0.003 \pm 0.115 \,.
\end{aligned}
$$

The result for the inclusive distribution is in good agreement with previous results [19, 20], whereas the position of the maxima of the flavour dependent ξ_p distribution is reported here for the first time. Part of the systematic uncertainties cancel when the ratio of the flavour dependent results to the inclusive result is taken:

$$
\begin{aligned}
\xi_0^{\mathrm{uds}}/\xi_0^{\mathrm{incl}} &= 1.023 \pm 0.017 \pm 0.028 \\
\xi_0^{\mathrm{c}}/\xi_0^{\mathrm{incl}} &= 0.993 \pm 0.044 \pm 0.082 \\
\xi_0^{\mathrm{b}}/\xi_0^{\mathrm{incl}} &= 0.971 \pm 0.003 \pm 0.022 \,.
\end{aligned}
$$

Another indication for a flavour dependence of the ξ_p distribution is given by the differences of the shape of the distributions in figure 3.

In Fig. 4, the total and the flavour dependent fragmentation functions are compared with results from other experiments at the same centre-of-mass energy. There is good agreement with [5] where the $\mathrm{D}^{*+} \to \mathrm{K}^- \pi^+ \pi^+$ decay was used as well, but a different b tagging method and a different correction procedure was applied. Also the quoted systematic uncertainty is similar in size with the exception of the high momentum region, where the uncertainty in [5] is smaller than in this paper. However, a direct comparison of the systematic errors is difficult since the error sources dominating the systematic uncertainty in the high momentum region in this paper (Table 7) are not explicitly considered in [5]. Also in Fig. 4, the results are shown to be consistent with the Jetset 7.4 expectation while the Herwig 5.9 Monte Carlo program [25][4] fails to describe fully the b fragmentation function.

The measurement of the total fragmentation function in comparison to measurements at lower energies [26] and at centre-of-mass energies between 130 GeV and 161 GeV [2, 17] is shown in Fig. 5. Apart from the lowest x_p region, there is good agreement with the Jetset 7.4 prediction (solid line) despite the fact that the parameters used in Jetset 7.4 were optimised to describe data at the Z^0 resonance. In the highest x_p bin, the difference between the total fragmentation function measured at $\sqrt{s} = 14.0$ GeV and at $\sqrt{s} = 161$ GeV is of the same order of magnitude as the difference between uds and b fragmentation function at $\sqrt{s} = 91.2$ GeV. Observing the good agreement between data and the Jetset 7.4 prediction of the $\sqrt{s}$ dependence of the total fragmentation function and of the flavour dependent fragmentation functions at $\sqrt{s} = 91.2$ GeV, we can use Jetset to estimate the effect of the change of the

---

[4]The parameter set used was the same as in [21] for Herwig 5.8, except for the value of the cluster mass cutoff CLMAX which has been increased from 3.40 GeV/c^2 to 3.75 GeV/c^2. Alternatively, studies were done with the default parameter set of the Herwig Monte Carlo program. But in this case, even the inclusive fragmentation function fails to describe the data.

flavour mix to the apparent scaling violation. In Fig. 5, the Jetset 7.4 prediction is shown when the flavour mix at all centre-of-mass energies was forced to be the same as the flavour mix at $\sqrt{s} = 18$ GeV. Although this fixed flavour mix is very different from that at at the Z^0 peak and the flavour dependent fragmentation functions differ significantly, the changes on the total fragmentation function at $\sqrt{s} = 91.2$ GeV are of the order of only two to four percent. This is due to a cancellation of the effect of an increased b contribution and a decreased c contribution at centre-of-mass energies close to the Z^0 resonance.

Comparing the positions of the maxima, ξ_0, of the ξ_p distribution, the flavour dependence is less pronounced than for the fragmentation function at high x_p. The values for ξ_0 at $\sqrt{s} = 14.0$ GeV and $\sqrt{s} = 161$ GeV differ by almost a factor of two, while the difference between the flavour dependent results at $\sqrt{s} = 91.2$ GeV is one order of magnitude smaller. Like in the case of the fragmentation functions, an increased b contribution and a simultaneously decreased c contribution leads to cancellations when comparing low energy measurements and results at the Z^0 peak. This is expected on the basis of simulations where the ξ_0 obtained for the flavour mixture at $\sqrt{s} = 91.2$ GeV and at $\sqrt{s} = 18.0$ GeV differ by less than one percent.

7   Conclusions

Flavour dependent fragmentation functions in $Z^0 \rightarrow q\bar{q}$ events have been measured separately for bottom, charm and light (uds) quarks and as well as for all flavours together. These measurements are based on OPAL data recorded between 1990 and 1995. Event samples with different flavour compositions were formed using reconstructed $D^{*\pm}$ mesons and secondary vertices in jets. The charged particle momentum spectrum has been studied in the event hemisphere opposite to the tag. A simultaneous fit was performed to extract the flavour dependent x_p distribution as well as the flavour dependent ξ_p distribution.

The fragmentation function for b quarks is significantly softer than for uds quarks. The fragmentation functions are well described by the Jetset 7.4 Monte Carlo program while Herwig 5.9 fails to describe fully the b fragmentation function.

For the first time, flavour dependent ξ_p distributions have been studied. The flavour dependence of the position of the maximum has been determined and was found to be small compared with the differences of this value at different centre-of-mass energies.

Acknowledgements

References

[1] DELPHI Collaboration, P.Abreu *et al.*, Phys. Lett. **B311** (1993) 408;
P.Nason and B.R.Webber, Nucl. Phys. **421** (1994) 473.

[2] OPAL Collaboration, K.Ackerstaff *et al.*, Z. Phys. **C75** (1997) 193.

[3] C.P.Fong and B.R.Webber, Nucl. Phys. **B355** (1991) 54.

[4] ALEPH Collaboration, D.Buskulic *et al.*, Phys. Lett. **B357** (1995) 487.

[5] DELPHI Collaboration, P.Abreu *et al.*, Phys. Lett. **B398** (1997) 194.

[6] OPAL Collaboration, R.Akers *et al.*, Z. Phys. **C61** (1994) 209.

[7] OPAL Collaboration, G.Alexander *et al.*, Phys. Lett. **B352** (1995) 176.

[8] OPAL Collaboration, K.Ahmet *et al.*, Nucl. Instr. Meth. **A305** (1991) 275;
P.P.Allport *et al.*, Nucl. Instr. Meth. **A324** (1993) 34;
P.P.Allport *et al.*, Nucl. Instr. Meth. **A346** (1994) 476.

[9] OPAL Collaboration, G.Alexander *et al.*, Z. Phys. **C52** (1991) 175.

[10] T.Sjöstrand, Comp. Phys. Comm. **39** (1986) 347;
T.Sjöstrand, Comp. Phys. Comm. **82** (1994) 74.

[11] OPAL Collaboration, G.Alexander *et al.*, Z. Phys. **C69** (1996) 543.

[12] J.Allison *et al.*, Nucl. Instr. Meth. **A317** (1992) 47.

[13] OPAL Collaboration, M.Z.Akrawy *et al.*, Phys. Lett. **B235** (1990) 389.

[14] OPAL Collaboration, K.Ackerstaff *et al.*, Z. Phys. **C74** (1997) 1.

[15] OPAL Collaboration, R.Akers *et al.*, Z. Phys. **C67** (1995) 27.

[16] M.H.Seymour, Nucl. Phys. **B436** (1995) 163.

[17] OPAL Collaboration, G.Alexander *et al.*, Z. Phys. **C72** (1996) 191.

[18] Yu.L.Dokshitzer, V.A.Khoze, A.H.Müller and S.I.Troyan: Basics of perturbative QCD.
Edition Frontières (1991);
V.A.Khoze, Yu.L.Dokshitzer and S.I.Troyan: Int. J. Mod. Phys. **A7** (1992) 1875.

[19] OPAL Collaboration, M.Z.Akrawy *et al.*, Phys. Lett. **B247** (1990) 617;
L3 Collaboration, B.Adeva *et al.*, Phys. Lett. **B259** (1991) 199.

[20] ALEPH Collaboration, R.Barate *et al.*, Phys. Rep. **294** (1998) 1;
DELPHI Collaboration, P.Abreu *et al.*, Z. Phys. **C73** (1996) 11.

[21] OPAL Collaboration, G.Alexnder *et al.*, Z. Phys. **C69** (1996) 543.

[22] ALEPH Collaboration, D.Buskulic *et al.*, Phys. Lett. **B384** (1996) 353.

[23] OPAL Collaboration, R.Akers *et al.*, Z. Phys. **C68** (1995) 203.

[24] SLD Collaboration, K.Abe *et al.*, Phys. Lett. **B386** (1996) 475.

[25] G.Marchesini *et al.*, Comp. Phys. Comm. **67** (1992) 465.

[26] TASSO Collaboration, W.Braunschweig *et al.*, Z. Phys. **C47** (1990) 187;
TPC Collaboration, H.Ahiara *et al.*, Phys. Rev. Lett. **61** (1988) 1263;
MARK II Collaboration, A.Peterson *et al.*, Phys. Rev. **D37** (1988) 1;
AMY Collaboration, Y.K.Li *et al.*, Phys. Rev. **D41** (1990) 2675;
HRS Collaboration, D.Bender *et al.*, Phys. Rev. **D31** (1985) 1 (results were scaled using
the multiplicity measurement in HRS Collaboration, M.Derrick *et al.*, Phys. Rev. **D34**
(1986) 3304).

[27] MARK II Collaboration, G.S.Abram *et al.*, Phys. Rev. Lett. **64** (1990) 1334.

x_p	$1/\sigma_{\mathrm{tot}} \cdot \mathrm{d}\sigma^h/\mathrm{d}x_p$		
	uds events	c events	b events
0.00–0.01	388. $\pm$ 5. $\pm$ 9.	413. $\pm$ 19. $\pm$ 18.	416. $\pm$ 1. $\pm$ 8.
0.01–0.02	390. $\pm$ 5. $\pm$ 10.	381. $\pm$ 17. $\pm$ 11.	447. $\pm$ 1. $\pm$ 8.
0.02–0.03	241. $\pm$ 4. $\pm$ 7.	287. $\pm$ 13. $\pm$ 8.	300. $\pm$ 1. $\pm$ 7.
0.03–0.04	176. $\pm$ 3. $\pm$ 5.	178. $\pm$ 11. $\pm$ 6.	215. $\pm$ 1. $\pm$ 5.
0.04–0.05	122.6$\pm$ 2.7 $\pm$ 3.9	159. $\pm$ 10. $\pm$ 5.	160.7 $\pm$ 0.6 $\pm$ 4.1
0.05–0.06	95.7 $\pm$ 2.2 $\pm$ 2.9	116. $\pm$ 8. $\pm$ 4.	126.1 $\pm$ 0.5 $\pm$ 3.4
0.06–0.07	79.3 $\pm$ 1.9 $\pm$ 2.3	79. $\pm$ 7. $\pm$ 3.	101.4 $\pm$ 0.4 $\pm$ 2.7
0.07–0.08	65.0 $\pm$ 1.6 $\pm$ 1.7	61. $\pm$ 6. $\pm$ 2.	81.9 $\pm$ 0.4 $\pm$ 2.2
0.08–0.09	53.3 $\pm$ 1.6 $\pm$ 1.3	59. $\pm$ 6. $\pm$ 2.	68.9 $\pm$ 0.4 $\pm$ 1.9
0.09–0.10	43.3 $\pm$ 1.5 $\pm$ 1.0	53. $\pm$ 5. $\pm$ 2.	57.1 $\pm$ 0.3 $\pm$ 1.6
0.10–0.12	35.1 $\pm$ 0.9 $\pm$ 0.7	41.9 $\pm$ 3.2 $\pm$ 1.5	44.0 $\pm$ 0.2 $\pm$ 1.3
0.12–0.14	27.7 $\pm$ 0.7 $\pm$ 0.4	27.6 $\pm$ 2.6 $\pm$ 1.2	30.9 $\pm$ 0.2 $\pm$ 1.0
0.14–0.16	21.2 $\pm$ 0.7 $\pm$ 0.4	23.8 $\pm$ 2.4 $\pm$ 1.0	22.5 $\pm$ 0.1 $\pm$ 0.8
0.16–0.18	17.1 $\pm$ 0.6 $\pm$ 0.3	17.6 $\pm$ 2.0 $\pm$ 0.8	16.8 $\pm$ 0.1 $\pm$ 0.6
0.18–0.20	13.3 $\pm$ 0.6 $\pm$ 0.3	16.5 $\pm$ 1.9 $\pm$ 0.7	12.3 $\pm$ 0.1 $\pm$ 0.5
0.20–0.25	9.86 $\pm$ 0.26 $\pm$ 0.30	9.8 $\pm$ 0.9 $\pm$ 0.5	7.82 $\pm$ 0.05 $\pm$ 0.40
0.25–0.30	6.30 $\pm$ 0.19 $\pm$ 0.25	5.5 $\pm$ 0.7 $\pm$ 0.3	4.16 $\pm$ 0.04 $\pm$ 0.29
0.30–0.40	3.42 $\pm$ 0.09 $\pm$ 0.17	2.49 $\pm$ 0.31 $\pm$ 0.19	1.84 $\pm$ 0.02 $\pm$ 0.18
0.40–0.50	1.50 $\pm$ 0.05 $\pm$ 0.10	0.95 $\pm$ 0.19 $\pm$ 0.26	0.65 $\pm$ 0.01 $\pm$ 0.10
0.50–0.60	0.668$\pm$0.033$\pm$0.048	0.36 $\pm$ 0.11 $\pm$ 0.10	0.210 $\pm$ 0.006 $\pm$ 0.052
0.60–0.80	0.241$\pm$0.008$\pm$0.024	0.014$\pm$0.041$\pm$0.015	0.038 $\pm$ 0.001 $\pm$ 0.020
0.80–1.00	0.031$\pm$0.007$\pm$0.007	0.003$\pm$0.046$\pm$0.012	0.0040$\pm$0.0005$\pm$0.0035

Table 3: *Fragmentation functions of uds, c and b events. The first error is statistical, the second systematic.*

x_p	$1/\sigma_{\mathrm{tot}} \cdot \mathrm{d}\sigma^h/\mathrm{d}x_p$			
0.00–0.01	401.2	$\pm$	0.3	$\pm$	7.4
0.01–0.02	401.6	$\pm$	0.2	$\pm$	4.9
0.02–0.03	262.8	$\pm$	0.2	$\pm$	3.9
0.03–0.04	185.5	$\pm$	0.2	$\pm$	2.9
0.04–0.05	137.5	$\pm$	0.1	$\pm$	2.1
0.05–0.06	106.2	$\pm$	0.1	$\pm$	1.6
0.06–0.07	84.5	$\pm$	0.1	$\pm$	1.2
0.07–0.08	68.3	$\pm$	0.1	$\pm$	0.9
0.08–0.09	57.9	$\pm$	0.1	$\pm$	0.7
0.09–0.10	47.9	$\pm$	0.1	$\pm$	0.6
0.10–0.12	38.19	$\pm$	0.05	$\pm$	0.42
0.12–0.14	28.30	$\pm$	0.04	$\pm$	0.28
0.14–0.16	21.88	$\pm$	0.03	$\pm$	0.19
0.16–0.18	17.10	$\pm$	0.03	$\pm$	0.16
0.18–0.20	13.54	$\pm$	0.03	$\pm$	0.14
0.20–0.25	9.37	$\pm$	0.01	$\pm$	0.11
0.25–0.30	5.66	$\pm$	0.01	$\pm$	0.08
0.30–0.40	2.89	$\pm$	0.01	$\pm$	0.05
0.40–0.50	1.208	$\pm$	0.004	$\pm$	0.036
0.50–0.60	0.506	$\pm$	0.002	$\pm$	0.018
0.60–0.80	0.153	$\pm$	0.001	$\pm$	0.012
0.80–1.00	0.0199	$\pm$	0.0003	$\pm$	0.0044

Table 4: *Inclusive fragmentation function. The first error is statistical, the second systematic.*

ξ_p	$1/\sigma_{\mathrm{tot}} \cdot \mathrm{d}\sigma^h/\mathrm{d}\xi_p$		
	uds events	c events	b events
0.0–0.2	0.024±0.006±0.006	0.002±0.147±0.005	0.0034±0.0001±0.0027
0.2–0.4	0.114±0.003±0.011	0.005±0.123±0.008	$0.014 \pm 0.001 \pm 0.010$
0.4–0.6	0.277±0.009±0.025	$0.07 \pm 0.03 \pm 0.06$	$0.066 \pm 0.002 \pm 0.023$
0.6–0.8	0.529±0.016±0.032	$0.20 \pm 0.06 \pm 0.07$	$0.188 \pm 0.004 \pm 0.034$
0.8–1.0	$0.86 \pm 0.02 \pm 0.05$	$0.52 \pm 0.08 \pm 0.11$	$0.40 \pm 0.01 \pm 0.05$
1.0–1.2	$1.31 \pm 0.03 \pm 0.06$	$0.84 \pm 0.12 \pm 0.12$	$0.71 \pm 0.01 \pm 0.07$
1.2–1.4	$1.76 \pm 0.05 \pm 0.07$	$1.43 \pm 0.16 \pm 0.15$	$1.15 \pm 0.01 \pm 0.07$
1.4–1.6	$2.22 \pm 0.06 \pm 0.06$	$2.10 \pm 0.20 \pm 0.14$	$1.74 \pm 0.01 \pm 0.09$
1.6–1.8	$2.70 \pm 0.07 \pm 0.06$	$2.88 \pm 0.24 \pm 0.18$	$2.49 \pm 0.02 \pm 0.10$
1.8–2.0	$3.06 \pm 0.08 \pm 0.09$	$3.89 \pm 0.29 \pm 0.29$	$3.41 \pm 0.02 \pm 0.08$
2.0–2.2	$3.76 \pm 0.09 \pm 0.11$	$3.70 \pm 0.31 \pm 0.34$	$4.30 \pm 0.02 \pm 0.13$
2.2–2.4	$4.03 \pm 0.10 \pm 0.13$	$4.77 \pm 0.35 \pm 0.31$	$5.19 \pm 0.02 \pm 0.11$
2.4–2.6	$4.48 \pm 0.10 \pm 0.18$	$5.32 \pm 0.37 \pm 0.45$	$5.98 \pm 0.02 \pm 0.15$
2.6–2.8	$5.12 \pm 0.11 \pm 0.16$	$4.83 \pm 0.37 \pm 0.21$	$6.46 \pm 0.03 \pm 0.15$
2.8–3.0	$5.22 \pm 0.12 \pm 0.17$	$6.39 \pm 0.41 \pm 0.31$	$6.92 \pm 0.03 \pm 0.15$
3.0–3.2	$5.26 \pm 0.13 \pm 0.19$	$7.89 \pm 0.48 \pm 0.37$	$7.19 \pm 0.03 \pm 0.16$
3.2–3.4	$6.24 \pm 0.12 \pm 0.21$	$5.48 \pm 0.43 \pm 0.40$	$7.37 \pm 0.03 \pm 0.17$
3.4–3.6	$6.02 \pm 0.12 \pm 0.20$	$6.90 \pm 0.44 \pm 0.36$	$7.49 \pm 0.03 \pm 0.17$
3.6–3.8	$5.89 \pm 0.13 \pm 0.26$	$7.12 \pm 0.45 \pm 0.74$	$7.49 \pm 0.03 \pm 0.16$
3.8–4.0	$6.04 \pm 0.12 \pm 0.20$	$6.50 \pm 0.43 \pm 0.40$	$7.26 \pm 0.03 \pm 0.16$
4.0–4.2	$5.85 \pm 0.13 \pm 0.20$	$6.24 \pm 0.46 \pm 0.49$	$6.93 \pm 0.03 \pm 0.14$
4.2–4.4	$5.58 \pm 0.11 \pm 0.14$	$5.67 \pm 0.40 \pm 0.35$	$6.32 \pm 0.03 \pm 0.09$
4.4–4.6	$5.15 \pm 0.11 \pm 0.09$	$4.84 \pm 0.40 \pm 0.16$	$5.76 \pm 0.03 \pm 0.08$
4.6–4.8	$4.21 \pm 0.12 \pm 0.24$	$5.76 \pm 0.41 \pm 0.80$	$4.91 \pm 0.02 \pm 0.05$
4.8–5.0	$3.99 \pm 0.10 \pm 0.14$	$3.35 \pm 0.36 \pm 0.43$	$4.24 \pm 0.02 \pm 0.07$
5.0–5.2	$2.94 \pm 0.10 \pm 0.15$	$3.34 \pm 0.33 \pm 0.45$	$3.30 \pm 0.02 \pm 0.06$
5.2–5.4	$2.14 \pm 0.10 \pm 0.12$	$3.22 \pm 0.34 \pm 0.40$	$2.54 \pm 0.02 \pm 0.06$
5.4–5.6	$1.93 \pm 0.08 \pm 0.13$	$1.36 \pm 0.28 \pm 0.32$	$1.92 \pm 0.02 \pm 0.09$
5.6–5.8	$1.43 \pm 0.09 \pm 0.23$	$0.78 \pm 0.32 \pm 0.62$	$1.42 \pm 0.03 \pm 0.16$

Table 5: $\xi_p = \ln(1/x_p)$ distribution of uds, c and b events. The first error is statistical, the second systematic.

ξ_p	$1/\sigma_{\mathrm{tot}} \cdot \mathrm{d}\sigma^h/\mathrm{d}\xi_p$
0.0–0.2	$0.0153 \pm 0.0003 \pm 0.0035$
0.2–0.4	$0.071 \pm 0.001 \pm 0.006$
0.4–0.6	$0.191 \pm 0.001 \pm 0.008$
0.6–0.8	$0.392 \pm 0.001 \pm 0.011$
0.8–1.0	$0.693 \pm 0.002 \pm 0.018$
1.0–1.2	$1.087 \pm 0.002 \pm 0.021$
1.2–1.4	$1.556 \pm 0.003 \pm 0.025$
1.4–1.6	$2.082 \pm 0.003 \pm 0.028$
1.6–1.8	$2.674 \pm 0.004 \pm 0.028$
1.8–2.0	$3.272 \pm 0.004 \pm 0.032$
2.0–2.2	$3.866 \pm 0.005 \pm 0.036$
2.2–2.4	$4.403 \pm 0.005 \pm 0.044$
2.4–2.6	$4.96 \pm 0.01 \pm 0.06$
2.6–2.8	$5.39 \pm 0.01 \pm 0.07$
2.8–3.0	$5.82 \pm 0.01 \pm 0.08$
3.0–3.2	$6.15 \pm 0.01 \pm 0.10$
3.2–3.4	$6.38 \pm 0.01 \pm 0.11$
3.4–3.6	$6.52 \pm 0.01 \pm 0.12$
3.6–3.8	$6.48 \pm 0.01 \pm 0.10$
3.8–4.0	$6.41 \pm 0.01 \pm 0.12$
4.0–4.2	$6.17 \pm 0.01 \pm 0.09$
4.2–4.4	$5.75 \pm 0.01 \pm 0.06$
4.4–4.6	$5.24 \pm 0.01 \pm 0.04$
4.6–4.8	$4.65 \pm 0.01 \pm 0.04$
4.8–5.0	$3.95 \pm 0.01 \pm 0.05$
5.0–5.2	$3.110 \pm 0.005 \pm 0.051$
5.2–5.4	$2.423 \pm 0.004 \pm 0.055$
5.4–5.6	$1.835 \pm 0.004 \pm 0.081$
5.6–5.8	$1.33 \pm 0.01 \pm 0.15$

Table 6: *Inclusive $\xi_p = \ln(1/x_p)$ distribution. The first error is statistical, the second systematic.*

Effect	inclusive		uds		c		b	
(1) Purities of sec. vertex samples	-	(-)	2.2	(4.0)	0.9	(1.5)	1.4	(6.5)
(2) Purities of D$^{*\pm}$ samples	-	(-)	0.2	(0.3)	0.5	(1.0)	< 0.1	(< 0.1)
(3) D$^{*\pm}$ selection	-	(-)	1.2	(1.8)	2.6	(4.2)	< 0.1	(0.1)
(4) Hemisphere correlation	-	(-)	0.2	(0.9)	0.4	(0.6)	0.3	(0.1)
(5) Correction procedure	< 0.1	(< 0.1)	0.8	(1.7)	1.0	(3.3)	1.7	(7.6)
(6) Track and event selection	1.5	(1.9)	1.5	(1.9)	1.5	(1.9)	1.5	(1.9)
Total systematic uncertainty	1.5	(1.9)	3.0	(5.2)	3.4	(6.0)	2.6	(10.2)
Total statistical uncertainty	0.1	(0.2)	2.3	(2.6)	6.7	(12.5)	0.4	(1.0)

Table 7: *Relative systematic and statistical uncertainties in percent on the results for $0.05 < x_p < 0.06$ $(0.3 < x_p < 0.4)$.*

Effect	inclusive	uds	c	b
(1) Purities of sec. vertex samples	-	1.4	0.8	1.3
(2) Purities of D$^{*\pm}$ samples	-	0.1	0.3	< 0.1
(3) D$^{*\pm}$ selection	-	0.6	2.1	< 0.1
(4) Hemisphere correlation	-	< 0.1	0.1	0.2
(5) Correction procedure	0.04	0.1	1.3	1.7
(6) Track and event selection	0.96	1.0	1.0	1.0
Total systematic uncertainty	0.96	1.8	2.8	2.4
Total statistical uncertainty	0.03	0.6	2.0	0.1

Table 8: *Relative systematic and statistical uncertainties in percent on the results for the mean value of the x_p distribution $\langle x_p \rangle$.*

Effect	inclusive	uds	c	b
(1) Purities of sec. vertex samples	-	0.6	0.1	0.2
(2) Purities of D$^{*\pm}$ samples	-	< 0.1	0.2	< 0.1
(3) D$^{*\pm}$ selection	-	0.5	2.0	< 0.1
(4) Hemisphere correlation	-	0.4	0.2	< 0.1
(5) Correction procedure	0.9	0.6	0.3	0.5
(6) Track and event selection	0.6	0.6	0.6	0.6
(7) Fit range and fit type	3.0	5.3	8.4	1.9
Total systematic uncertainty	3.1	5.4	8.7	2.1
Total statistical uncertainty	0.1	1.5	4.1	0.3

Table 9: *Relative systematic and statistical uncertainties in percent on the results for the position of the maximum of the ξ_p distribution, ξ_0.*
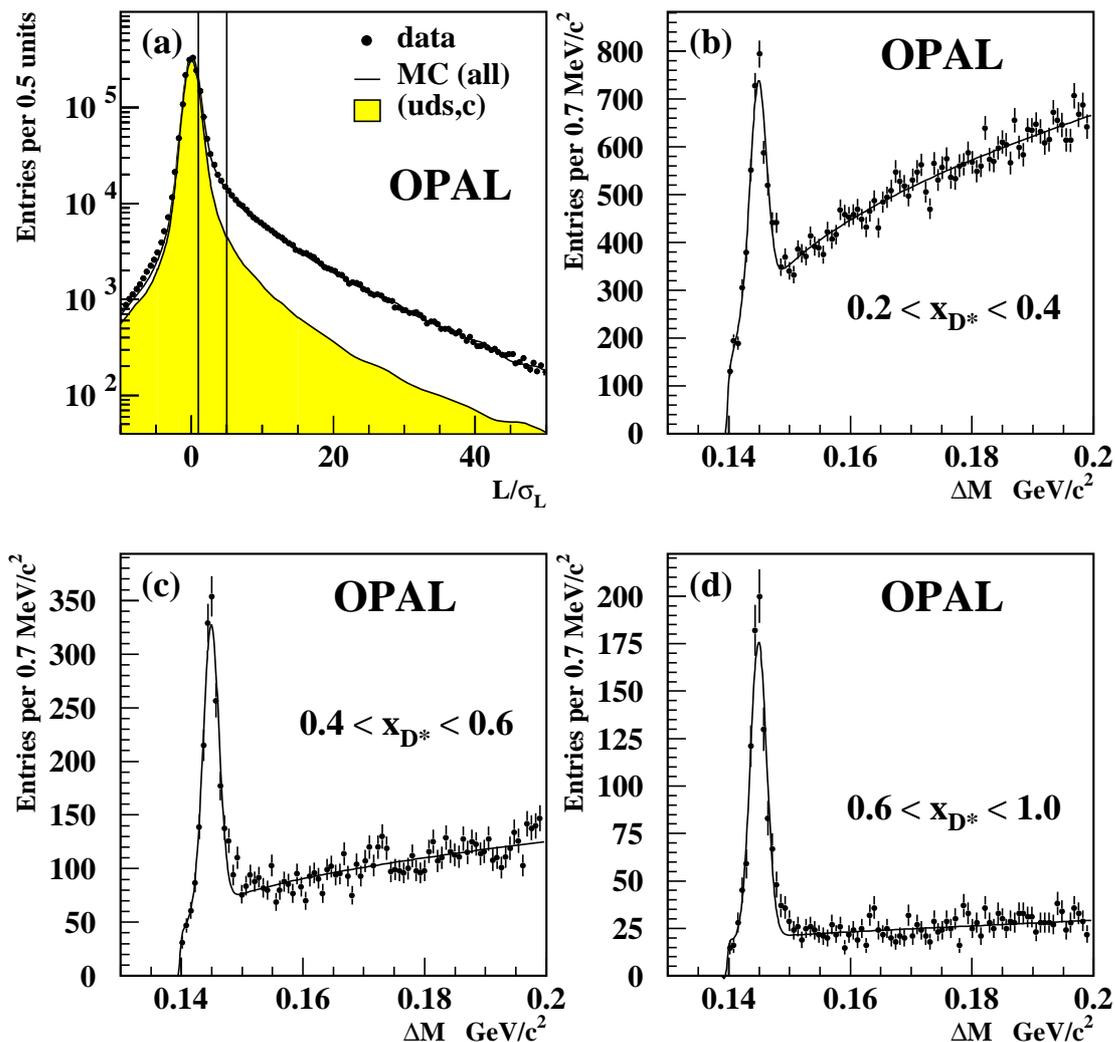
Figure 1: (a): The decay length significance distribution in data (symbols) and Monte Carlo (solid curve). The contribution from uds and from c quarks in the Monte Carlo distribution has been shaded. The boundaries of the three decay length significance bins used in this analysis: $-10 < L/\sigma_L < 1$, $1 < L/\sigma_L < 5$ and $5 < L/\sigma_L < 50$ are indicated by vertical lines. (b) to (d): The distribution of the mass difference of the $D^{*\pm}$ candidate and D^0 candidate in the three different x_{D*} bins. The symbols show the data while the solid lines are the results of the fits described in the text.
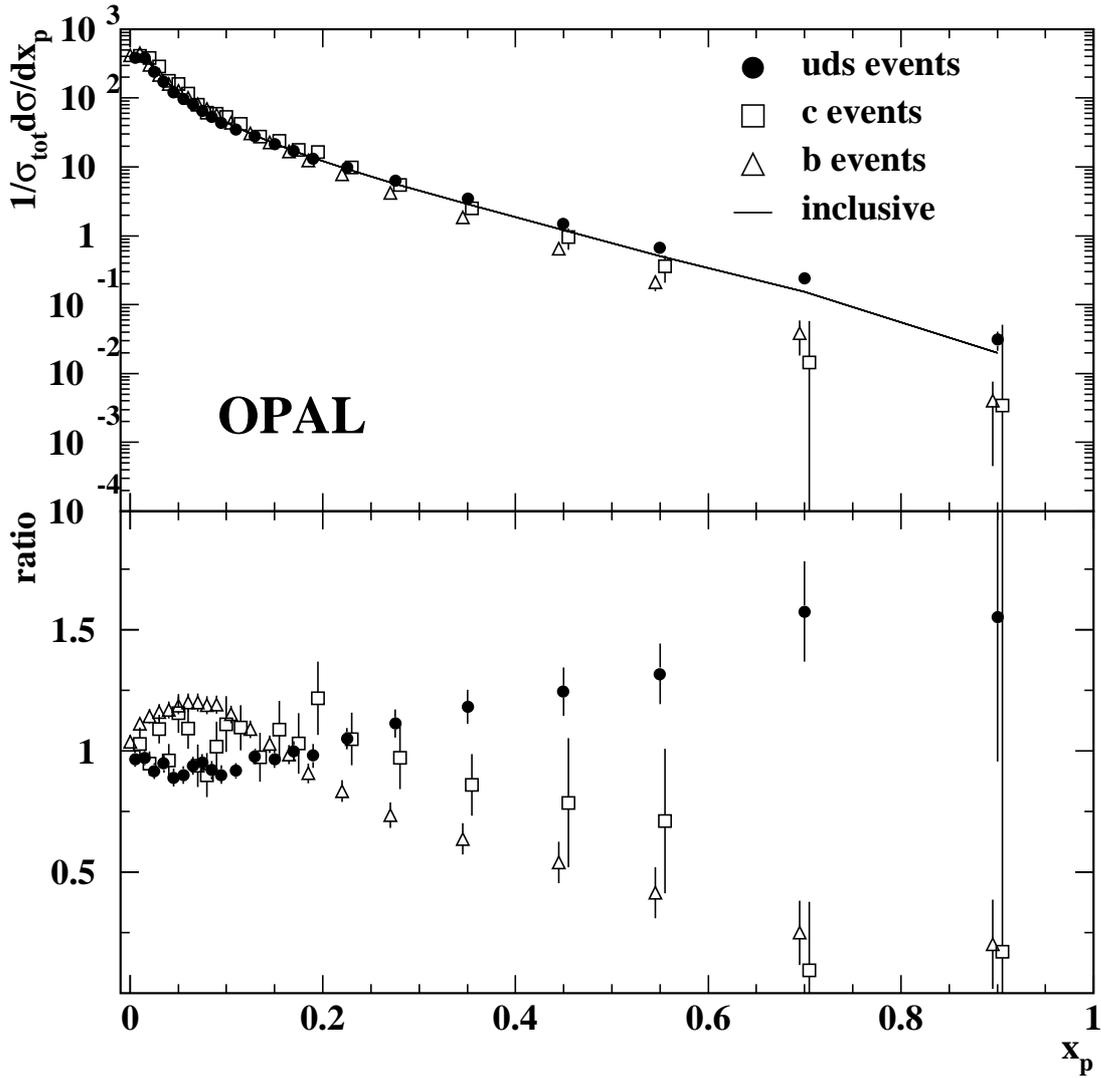
Figure 2: *The upper plot shows the measured fragmentation functions for uds events (filled symbols), c events (open squares) and b events (open triangles) as well as the inclusive fragmentation function (solid line). The lower plot shows the ratio of the flavour dependent fragmentation functions to the inclusive fragmentation function. The error bars include statistical and systematic uncertainties. The systematic uncertainties are correlated between bins as well as between flavours.*
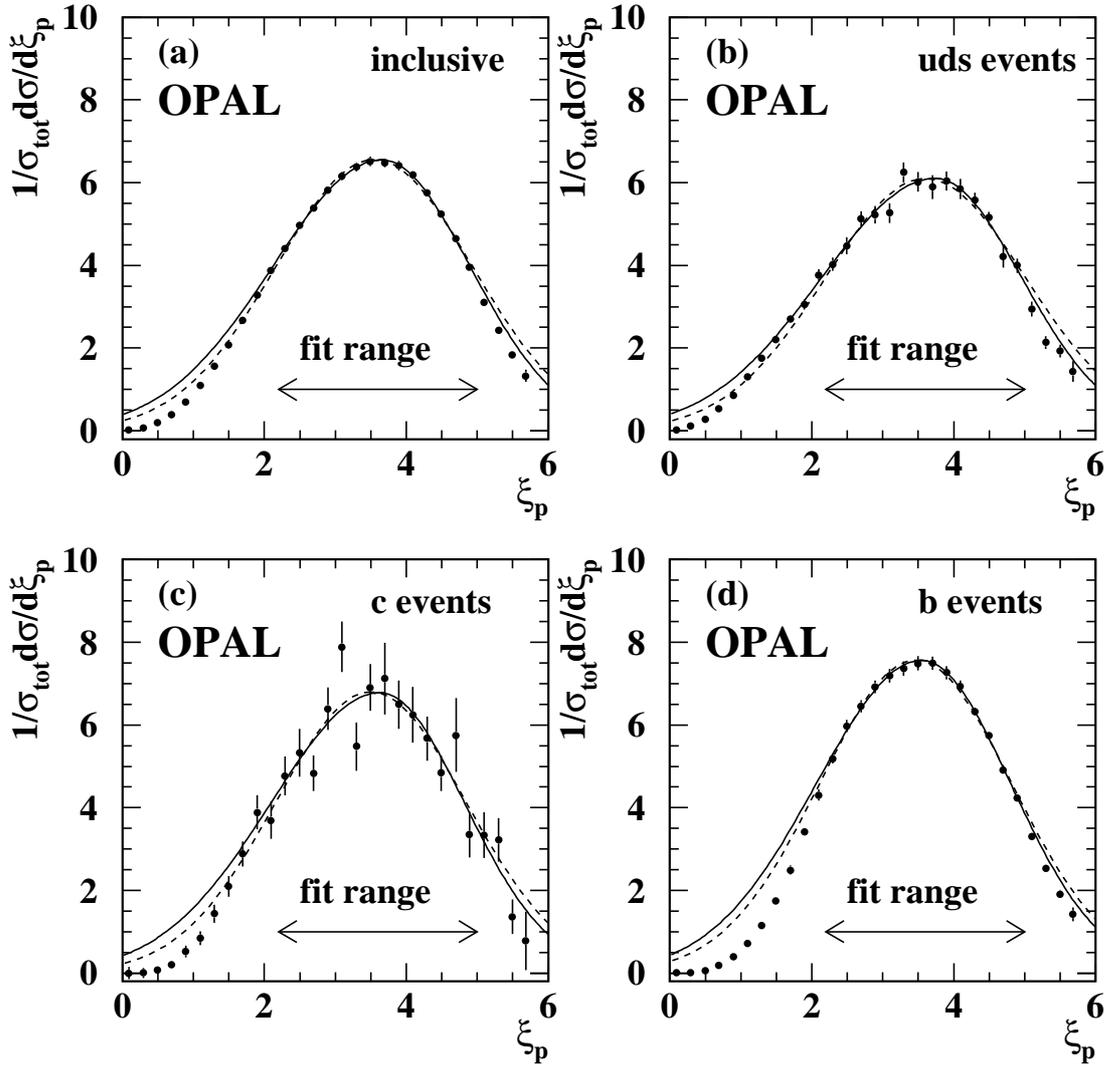
Figure 3: $\xi_p = \ln(1/x_p)$ distribution for (a) all events, (b) uds events, (c) c events and (d) b events. The solid lines show the results of the skewed Gaussian fitted to the distributions in the indicated fit range and the dashed lines show the results of a normal Gaussian fit. The error bars include statistical and systematic uncertainties.
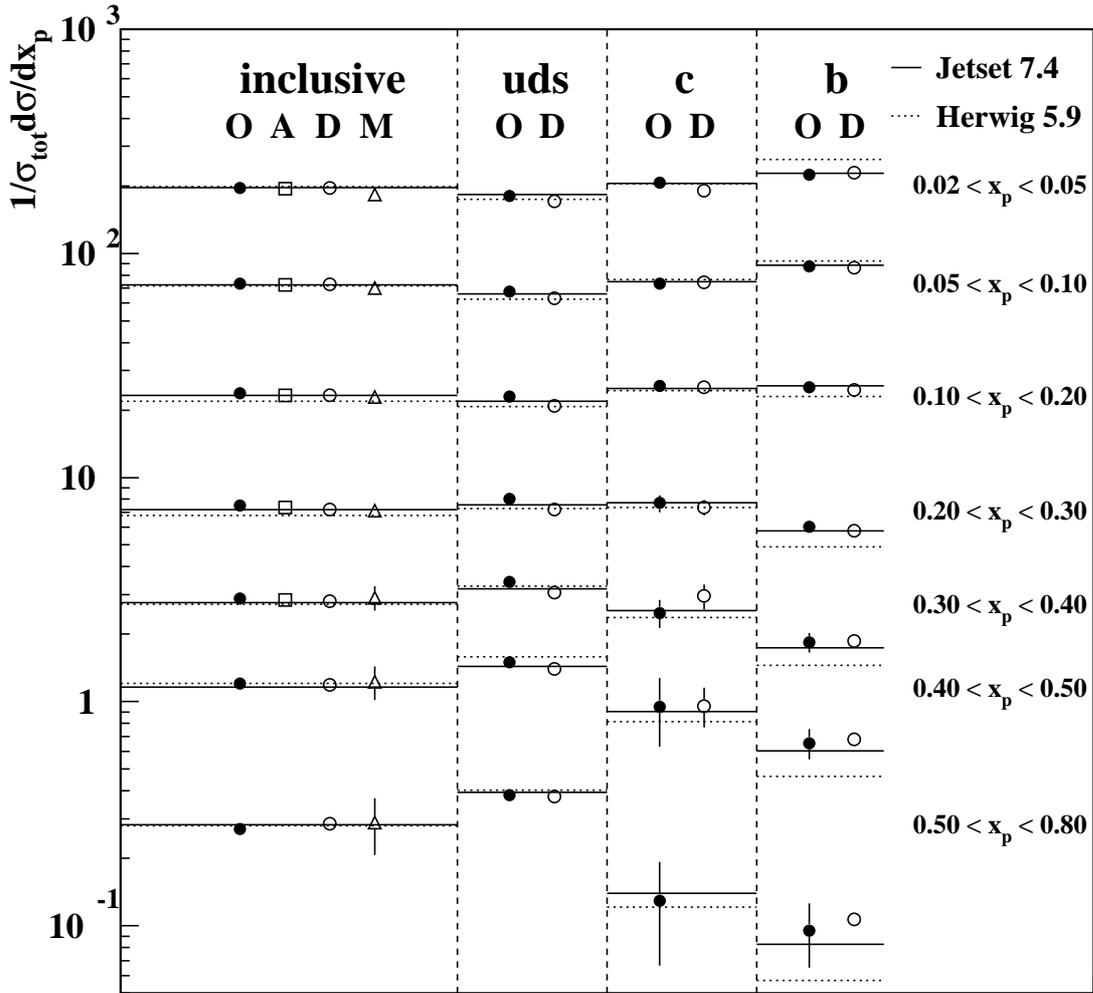
Figure 4: *Comparison of the results for the inclusive fragmentation function for this analysis (O) with results from ALEPH (A), DELPHI (D) and MARK II (M) at $\sqrt{s} = m_{Z^0}$ [20, 27] and of the flavour dependent fragmentation function with the results from DELPHI [5]. The error bars include statistical and systematic uncertainties. The Jetset 7.4 predictions for the fragmentation function are shown as full horizontal lines and the Herwig 5.9 predictions as dotted horizontal lines.*
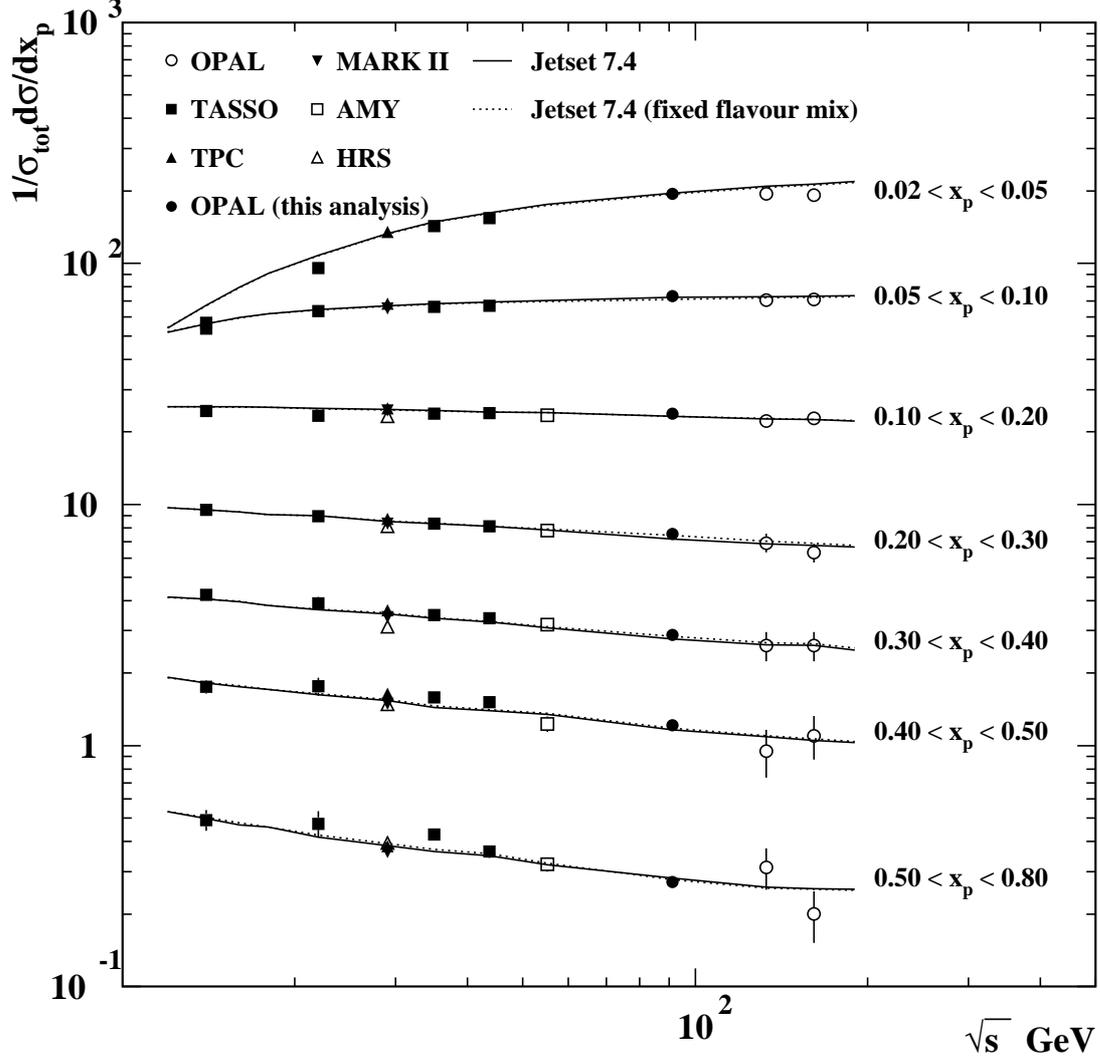
Figure 5: *Comparison of the results for the inclusive fragmentation function with results at different lower [26] and higher centre-of-mass energies [2, 17]. The error bars include statistical and systematic uncertainties. The solid lines show the Jetset 7.4 prediction, assuming the centre-of-mass energy dependence of the flavour composition as predicted by the electroweak theory. The dotted lines show the Jetset 7.4 prediction assuming for all energies the same flavour mix as at $\sqrt{s} = 18$ GeV. The dotted line is almost entirely hidden behind the full line and even at $\sqrt{s} = 91.2$ GeV, only a negligible difference between the two curves can be seen because the effect of an increased b contribution is compensated largely by the effect of a decreased c contribution.*